5B.4 Roles of the MJO in the development of Oceanic Kelvin waves and ENSO

Paul E. Roundy*
University at Albany
George N. Kiladis
NOAA Earth System Research Laboratory, Boulder, CO

1. Introduction

Oceanic Kelvin waves are a dominant mode of variability in the equatorial Pacific Ocean (e.g., Knox and Halpern 1982; Johnson and McPhaden 1993; Cravatte et al. 2003). In an observational study based on analysis of sea surface dynamic height data derived from the TAO (Tropical Atmosphere Ocean) array of buoys moored in the tropical Pacific (McPhaden 1995), Roundy and Kiladis (2006, hereafter RK06) showed systematic changes in the amplitudes and phase speeds of these waves during periods when dynamic height variance associated with Kelvin waves exceeds the long-term mean. They confirmed that the waves are primarily triggered by the Madden-Julian Oscillation (MJO, Enfield 1987; McPhaden et al. 1988; Madden and Julian 1994; Kessler et al. 1995; Kessler and Kleeman 2000; Shinoda and Hendon 2002; Zhang and Gottschalck 2002; Kutsuwada and McPhaden 2002), that they tend to attain their highest amplitudes during periods when the ocean is adjusting toward El Niño conditions, and that the wave phase speeds tend to decrease with time during periods of enhanced activity. The analysis of RK06 covered the period 1988-2005, when TAO data were plentiful enough to diagnose Kelvin wave phase. Though that dataset exceeds 15 years in length, it is arguably not sufficiently long to generalize results to other periods, because the El Niño/Southern Oscillation (ENSO) exhibits marked decadal scale variability in its amplitude.

Although Kelvin waves can only be effectively studied in the TAO dataset since after 1988, other datasets, including daily sea level observations from islands in the tropical Pacific and the coast of South America, reanalysis winds, and satellite measured outgoing longwave radiation (OLR) data are available for much longer periods. The purpose of this work is to support the development of a conference talk showing relationships between the MJO, Kelvin waves in the ocean, and ENSO, by describing the development of a reconstructed dynamic height dataset applicable to analyzing the behaviors of oceanic Kelvin waves since 1974, based on regression relationships between island sea level height records, OLR, and TAO dynamic height. This abstract emphasizes the development of the reconstructed dataset following a paper we submitted recently to the Journal of Climate (Roundy and Kiladis 2007), while the talk will emphasize application of the dataset to enhance understanding of interactions between the MJO, the waves, and ENSO.

2. Data

Dynamic height data were obtained from the Pacific Marine Environment Laboratory (PMEL) website (Http://www.pmel.noaa.gov), and were averaged from 2ºS to 2ºN. Daily sea level height data were obtained from the University of Hawaii Sea Level Center for the set of island and coastal locations in the tropical Pacific shown in Table 1. Dynamic height data from the TAO array were used as a basis for training regression models to reconstruct Kelvin wave signals. These data provide a convenient grid on which to reconstruct wave signals because buoys are positioned approximately every 15-degrees along the equator, whereas the island stations are scattered more randomly around the basin at various distances from the equator, with stations most concentrated in the region west of the dateline. East Pacific sea level sites are

*University at Albany, DEAS-ES351, Albany, NY 12222, roundy@atmos.albany.edu

limited to those at the Galapagos Islands and the coast of South America.

We linearly interpolated in time across periods of missing data shorter than 20 days, then filtered for periods of 20-120 days by using the least-squares fits of sine and cosine waves, except that sea level data from locations east of 150ºW were filtered for periods of 35-120 days to reduce the contributions of tropical instability waves (Contreras 2002) and because Kelvin waves tend to be characterized by lower frequencies there than farther west (RK06). Missing filtered TAO dynamic height data were then filled by regression as described in Section 3.

Zonal and meridional wind data from 1000 hPa were obtained from the NCEP/NCAR reanalysis. NOAA provided interpolated OLR data for the period June 1974 through December 2005 (Liebmann and Smith 1996). OLR and wind anomalies were obtained by removing the mean and the first three harmonics of the seasonal cycle (by Fourier methods). An index of East-Central Pacific intraseasonal OLR was constructed by filtering OLR data in the 20-120 day band and averaging the result over the region 115ºW to 225ºW and 2.5ºN to 10ºN.

3. Reconstruction

a. Overview

We used time filtering and regression to diagnose and reconstruct Kelvin wave signals. Regression models were constructed to fill in all values missing from the interpolated and filtered daily equatorial Kelvin wave dynamic height dataset between January 1, 1974 and December 31, 2005. *Selections* from all available equatorial TAO data and sea level observations from the sites listed in Table 1 were utilized simultaneously to predict the missing data except that data from the buoy at 137ºE were not used because they contributed to loss of skill across the western basin (see Section 4b). Two additional reconstructions starting with smaller subsets of the predictors were made for analyzing the skill of the method as described below. Equation (1) gives the form of the models used:

$$
\begin{aligned}
y = {} & a_0 + a_1 I_1 + a_2 I_1^2 + a_3 I_1^3 + \\
& a_4 \dot{I}_1 + a_5 \dot{I}_1^2 + a_6 \dot{I}_1^3 + \\
& \ldots + a_{6n+1} I_n + a_{6n+2} I_n^2 + \\
& a_{6n+3} I_n^3 + a_{6n+4} \dot{I}_n + a_{6n+5} \dot{I}_n^2 + , \\
& a_{6n+6} \dot{I}_n^3 + a_{6n+7} OLR + \\
& a_{6n+8} I_2 I_8 + a_{6n+9} I_7 I_{10} + \varepsilon
\end{aligned}
\qquad (1)
$$

where y is filtered TAO dynamic height data at a given equatorial buoy, I_n is a sea level or dynamic height time series from the nth station or buoy, and the a_x coefficients are regression parameters calculated by matrix inversion (e.g., Wilks 2006; Strang 1998). For convenience, the first 11 subscripts on I represent the station numbers listed in table 1. Power terms diagnose relationships that cross frequency bands, allowing modeling of relationships between time series of different shapes (e.g., Wilks 2006). These are important both because the frequency of the Kelvin waves tends to decrease toward the east (RK06) and because signals measured at stations farther from the equator tend to be dominated by frequencies lower than those of related processes on the equator. The dot over I represents the first finite time difference. These derivative terms, in combination with the others, help the model to diagnose the phase difference between the sea level data at a given station and the dynamic height y at a buoy. This matches the phases of waves in the reconstructed dynamic height data to those in TAO dynamic height. These are important both because the signal at each location is shifted in phase from that at every other location, and because dynamic height and sea level are not necessarily equivalent, even when measured at the same point. The OLR term is the East-Central Pacific OLR index described above, and it is included because no sea level data are available in the region and because RK06 showed that Kelvin waves are occasionally coupled to atmospheric convection across

the region during El Niño. Cross product terms help the model resolve spatial scales and phase speeds of waves crossing portions of the East Pacific where sea-level data are not available. ε represents the model residuals.

Additional predictors are derived by lagging time series of sea level height and dynamic height in time. These terms improve the resolution of the reconstruction, especially during periods when many predictors are simultaneously missing but data are available within a short time before or after the missing point.

Several predictors are significantly correlated with each other (leading to overdetermination or overfitting). Such correlations, or colinearities, make the model coefficients difficult to resolve and prevent unique solutions from being found. Additionally, the total number of predictors exceeds 200. We eliminated colinearity reduced the number of predictors through the following process. Each predictor was first normalized by subtracting the mean and dividing by its standard deviation. An orthogonal basis for the set of normalized predictors was then found, following Roundy and Frank (2004) and RK2006. Next, the projections of each predictor onto the selected dynamic height time series were found by taking the vector dot product. These projections were sorted from minimum to maximum absolute values, and a cumulative sum of these absolute values was taken. The series of sums was then divided by the maximum sum, resulting in values increasing from zero to one. We then eliminated predictors associated with cumulative sum values of less than 0.2. This cutoff was determined by optimizing the skill of the reconstruction across the basin, relative to climatology in approximating observed anomalies. The method thus selects the subset of available predictors in equation (1) that produces the best overall fit to observations outside of the training set, following the methods in Section 3 b.

Different combinations of predictors were available at different times, so regression relationships were obtained for all combinations that occur. The normalization and orthogonalization procedure was performed for each subset of predictors. After applying the orthogonalization procedure, each missing value at each buoy longitude was filled by finding the appropriate set of regression coefficients relating the selected subset of available predictors to that buoy. The quantity returned by equation 1 after substituting predictor values appropriate for the missing value was then substituted for that value.

4. Results

a. Comparison of reconstructed and actual dynamic height

Figure 2 shows the observed dynamic height (panel a) and the second and third sets of reconstructed dynamic height discussed in Section 3 (panels b and c, respectively) during the 2002-2003 El Niño (compare Fig. 1 of RK06). Some phase shifts are evident between the three panels, but the general wave patterns seen in the TAO data are maintained by the reconstructions. Although the amplitudes of anomalies in the third reconstruction are generally smaller than those of corresponding anomalies in the first, a few low-amplitude anomalies in TAO data correspond to higher-amplitude reconstructed anomalies (e.g., February 2003). In general, the highest amplitude observed waves tend to be well described by both reconstructions. The decreasing phase speeds of successive waves documented by RK06 (especially early in the period) is evident in both reconstructions.

b. Consistency with winds during 1974-1988

Although reconstructed dynamic height prior to about 1988 cannot be effectively compared with TAO dynamic height at most buoys, they can be checked for consistency with surface wind data, because most intraseasonal Kelvin waves in the Pacific are forced by wind stress (e.g., Cravatte et al. 2003; Boulanger et al. 2003). Figure 3 shows the NCEP reanalysis 1000 hPa u

wind anomalies overlaid with contours of reconstructed dynamic height for the period September 1981 through mid-February 1983. In general, positive anomalies of reconstructed dynamic height (red contours) follow periods of westerly anomalies, and negative dynamic height anomalies follow periods of easterly anomalies. The timing of wave development relative to the wind bursts appears to be generally consistent with RK06. The December 1981 Kelvin wave has been considered by many as instrumental to the development of the 1982-1983 El Niño (e.g., Weickmann 1991), but this reconstruction suggests that intraseasonal Kelvin waves also developed March-April, June-July, and November 1982. Figure 4 shows contours of positive reconstructed dynamic height anomalies, with OLR shaded. Eastward-moving active convective anomalies associated with the MJO precede the development of Kelvin waves during April, May-June, and November.

Figure 5 shows the winds and reconstructed dynamic height for April 27, 1986 through September 9, 1987. All downwelling Kelvin waves suggested by positive (red) contours of reconstructed dynamic height are preceded by westerly wind bursts of varying amplitudes, and upwelling waves (blue contours) tend to be associated with easterly anomalies near their origination points. Higher amplitude dynamic height anomalies are usually associated with higher amplitude wind anomalies.

Figures 3 and 5 show Kelvin wave anomalies responding to changes in surface winds. These results suggest that westerly wind bursts tend to amplify downwelling waves and are associated with eastward propagation, whereas enhanced trade winds appear to attenuate downwelling waves and occasionally result in slower eastward propagation. Away from downwelling waves, easterly wind anomalies are associated with the development of upwelling waves. These results suggest that the reconstruction is consistent with the expected location and timing of Kelvin waves during the periods shown. Further analysis suggests similarly consistent relationships during other periods before 1988 as well (such as an active period during 1979), though the highest amplitude waves during the period 1974-1987 occur during the periods shown in Figs. 3 and 5.

5. Discussion

Dynamic height data filtered for the frequency band of oceanic Kelvin waves are reconstructed from sea level records for the period 1974-2002. Data reconstructed for a skill test are generally consistent with the filtered dynamic height during the period 1988-2003, and are consistent with the expected response to zonal wind anomalies during the period 1974-1987. Results suggest that intraseasonal Kelvin wave amplitudes during the period 1981-1983 were greater than suggested by the wind-forced model based reconstruction of Bergman et al. (2001).

Acknowledgements: Funding for this work was provided by the NOAA Office of Global Programs under grant GC01-351 to GNK and a start-up funds package to PER from the Research Foundation of the State University of New York. The TAO Project Office of NOAA/PMEL provided the mooring time series data. The University of Hawaii Sea Level Center provided sea level time series from island and coastal sites used in the reconstruction.

Works Cited

Boulanger, J.-P., S. Cravatte, and C. Menkes, 2003: Reflected and locally wind-forced interannual equatorial Kelvin waves in the western Pacific Ocean, *J. Geophys. Res.*, **108 (C10)**, 311, doi:10.1029/2002JC001760.

Bergman, J. W., H. H. Hendon, and K. M. Weickmann, 2001: Intraseasonal air-sea interactions at the onset of El Niño. *J. Climate*, **14**, 1702-1719.

Contreras, R. F., 2002: Long-term observations of tropical instability

waves. *J. Phys. Oceanog.* **32**, 2715-2722.

Cravatte, S., J. Picaut, and G. Eldin, 2003: Second and first baroclinic Kelvin modes in the equatorial Pacific at intraseasonal time scales. *J. Geophys. Res.* **108**, 22: 1-20.

Enfield, D.B., 1987: The intraseasonal oscillation in eastern Pacific sea levels: How is it forced? *J. Phys. Oceanogr.*, **17**, 1860-1876.

Johnson, E. S., and M. J. McPhaden, 1993: Structure of intraseasonal Kelvin waves in the equatorial Pacific Ocean. *J. Phys. Oceanogr.*, **23**, 608-625.

Kessler, W. S., M. J. McPhaden, and K. M. Weickmann, 1995: Forcing of intraseasonal Kelvin waves in the equatorial Pacific. *J. Geophys. Res.*, **100**(C6), 10613-10631.

Kessler, W. S., and R. Kleeman, 2000: Rectification of the Madden-Julian Oscillation into the ENSO cycle. *J. Climate*, **13**, 3560-3575.

Knox, R. A. and D. Halpern, 1982: Long range Kelvin wave propagation of transport variations in Pacific Ocean equatorial currents. *J. Mar. Res.*, **40**, suppl., 329-339.

Kutsuwada, K., and M. McPhaden, 2002: Intraseasonal variations in the upper equatorial Pacific Ocean prior to and during the 1997-1998 El Niño. *J. Phys. Oceanogr.*, **32**, 1133-1149.

Liebmann, B., and C. A. Smith, 1996: Description of a complete (interpolated) outgoing longwave radiation dataset. *Bull. Amer. Meteor. Soc.* **77**, 1275-1277.

Madden, R. A., and P. R. Julian, 1994: Observations of the 40-50-day tropical oscillation-A review. *Mon. Wea. Rev.*, **122**, 814-837.

McPhaden, M. J., 1995: TAO array is completed. *Bull. Amer. Meteor. Soc.*, **76**, 739-741.

McPhaden, M. J., H. P. Freitag, S.P. Hayes, and B.A. Taft, 1988: The response of the equatorial Pacific Ocean to a westerly wind burst in May 1986. *J. Geophys. Res.*, **93**, 10589-10603.

Roundy, P. E., and W. M. Frank, 2004: Effects of low-frequency wave interactions on intraseasonal oscillations. *J. Atmos. Sci.*, 61, 3025-3040.

Roundy, P. E., and G. N. Kiladis, 2006: Observed relationships between oceanic Kelvin waves and atmospheric forcing. *J. Climate*. **19**, 5253-5272.

Roundy, P. E., and G. N. Kiladis, 2007: Analysis of a reconstructed oceanic Kelvin wave dynamic height dataset for the period 1974-2005. Submitted to *J. Climate* Fall 2006.

Shinoda, T. and H. H. Hendon, 2002: Rectified wind forcing and latent heat flux produced by the Madden-Julian Oscillation. *J. Climate*, **15**, 3500-3507.

Strang, G., 1995: *Linear Algebra and its Application.* Harcourt Brace & Company, San Diego, 535 pp.

Weickmann, K. M., 1991: El Niño Southern Oscillation and Madden-Julian (30-60-day) oscillations during 1981-1982. *J. Geophys. Res.*, **96**, Supplement, 3187-3195.

Wilks, D. S., 2006: Statistical Methods in the Atmospheric Sciences, an Introduction. Academic Press. 627pp.

Zhang, C., and J. Gottschalck, 2002: SST anomalies of ENSO and the Madden-Julian Oscillation in the equatorial Pacific. *J. Climate*, **15**, 2429-2445.

Station Name	Latitude	Longitude	Start Date	End Date	Completeness
1. Malakal-B	7º-20'N	134º-28'E	1969	2003	95%
2. Rabaul	4º-12'S	152º-11'E	1966	1997	85%
3. Kapingamarangi	1º-6'N	154º-47'E	1978	2001	92%
4. Pohnpei-B	6º-59'N	158º-15'E	1974	2003	98%
5. Kwajalein	8º44'N	167º-44'E	1946	2003	98%
6. Kanton	2º-49'S	171º-43'W	1972	2001	93%
7. Penrhyn	8º-59'S	158º-3'W	1977	2001	95%
8. Christmas-B	1º-6'N	157º-2'W	1974	2003	96%
9. Santa Cruz	0º-45'S	90º-19'W	1978	2003	95%
10. La Libertad	2º-12'S	80º-55'W	1949	2001	97%
11. Tumaco	1º-50'N	78º-44'W	1951	2000	86%

Table 1: Statistics of the daily sea level stations used in the reconstruction.

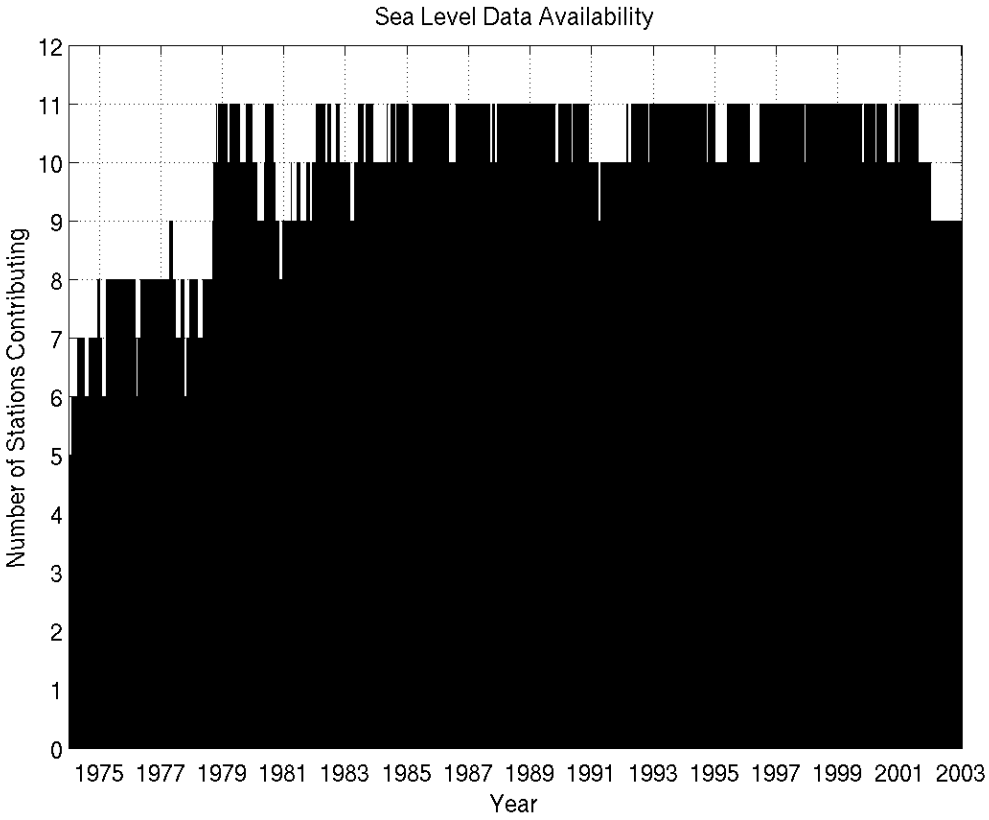

Figure 1 Number of sea level stations having data available during each day of the 1974-2002 period. The count was made after linearly interpolating over periods of missing data shorter than 20 days.

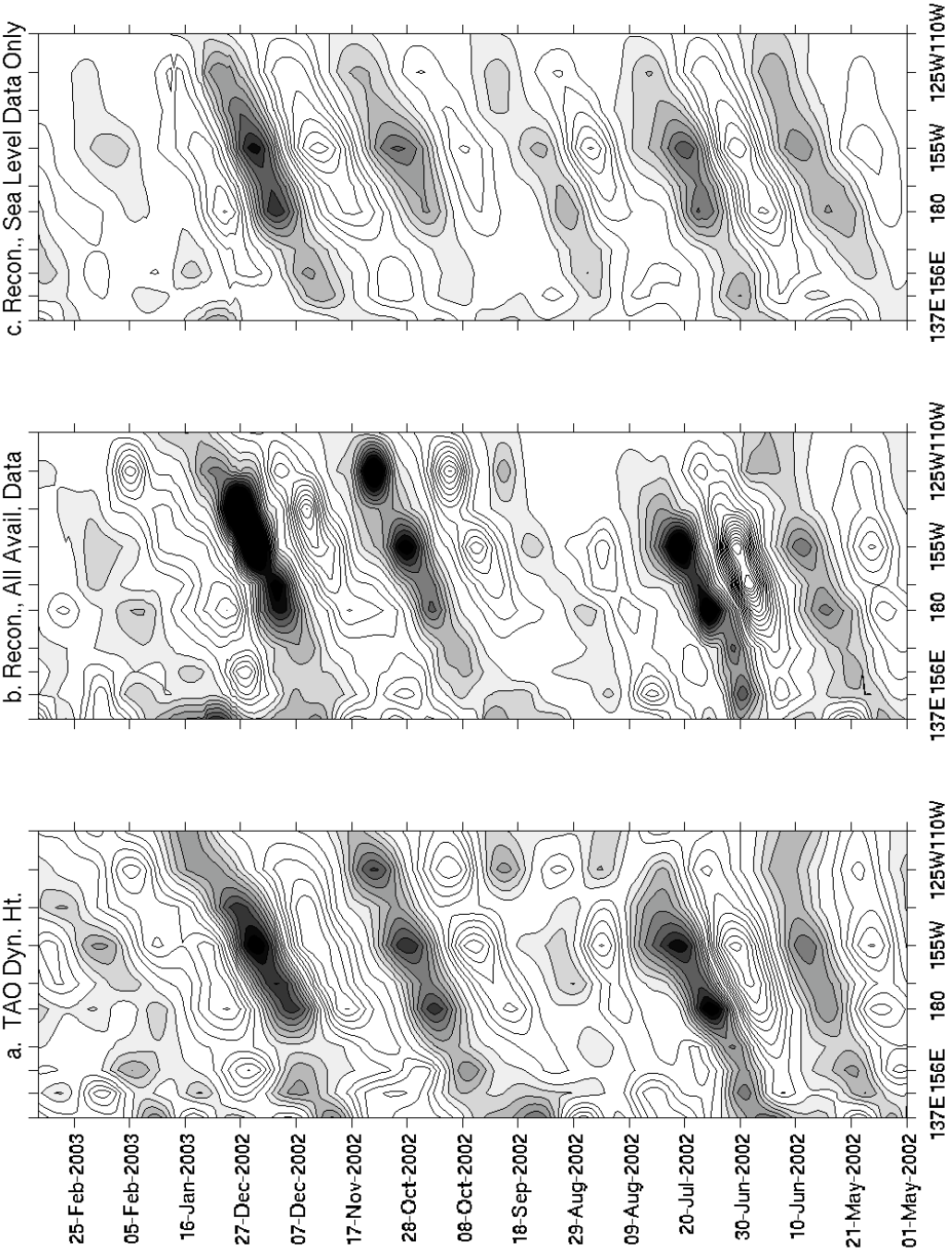

Figure 2 Reconstructed and observed 20-100 day band dynamic height. a. Verification filtered directly from TAO data. b. Reconstructed using all available data except from the location being reconstructed. c. Reconstructed using only sea level station data and the East Central Pacific OLR index.

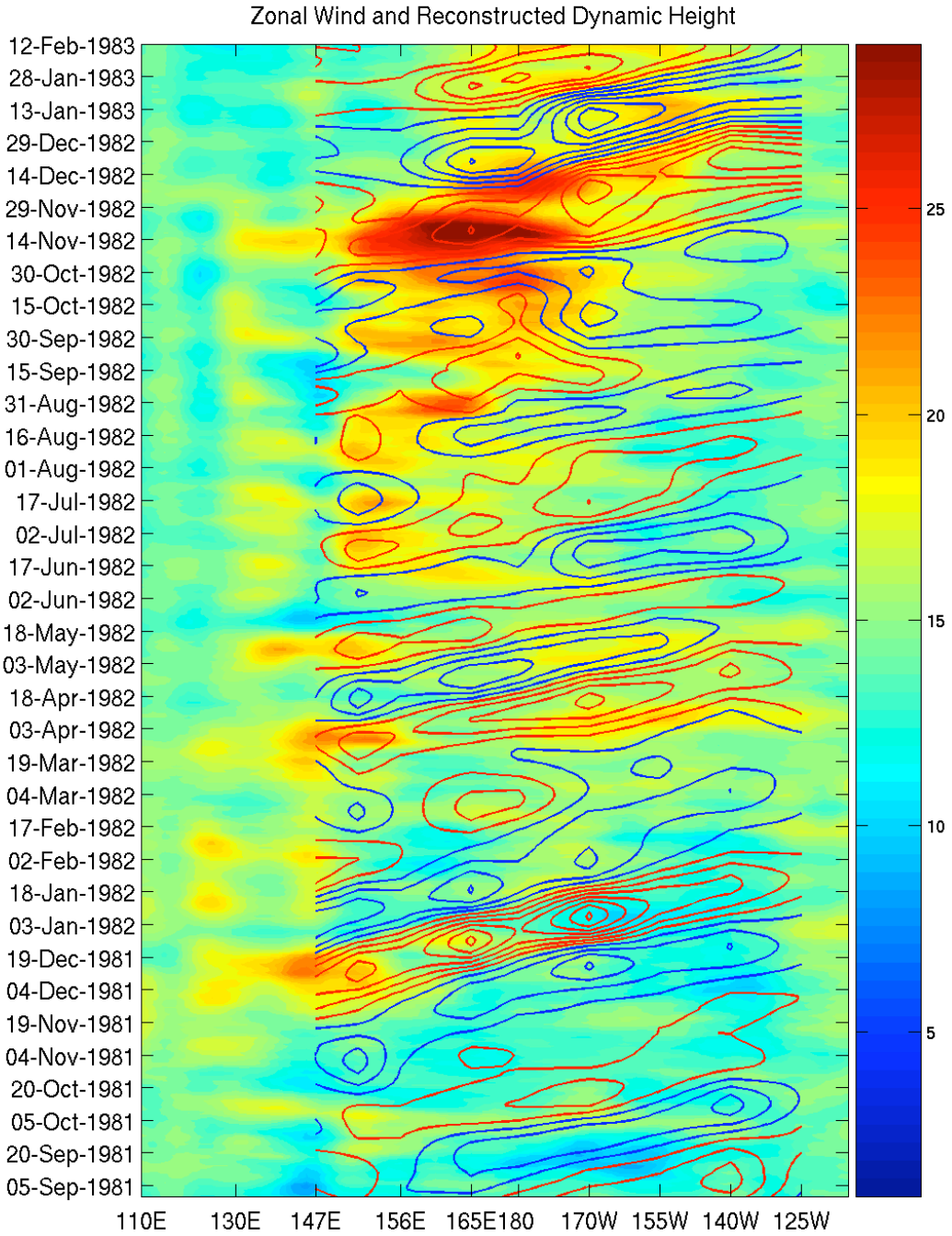

Figure 3 Zonal wind anomalies (ms^{-1}, shading), plotted with contours of reconstructed dynamic height (positive in red and negative in blue, given ever 2 cm with the minimum contours at +/-1 cm.

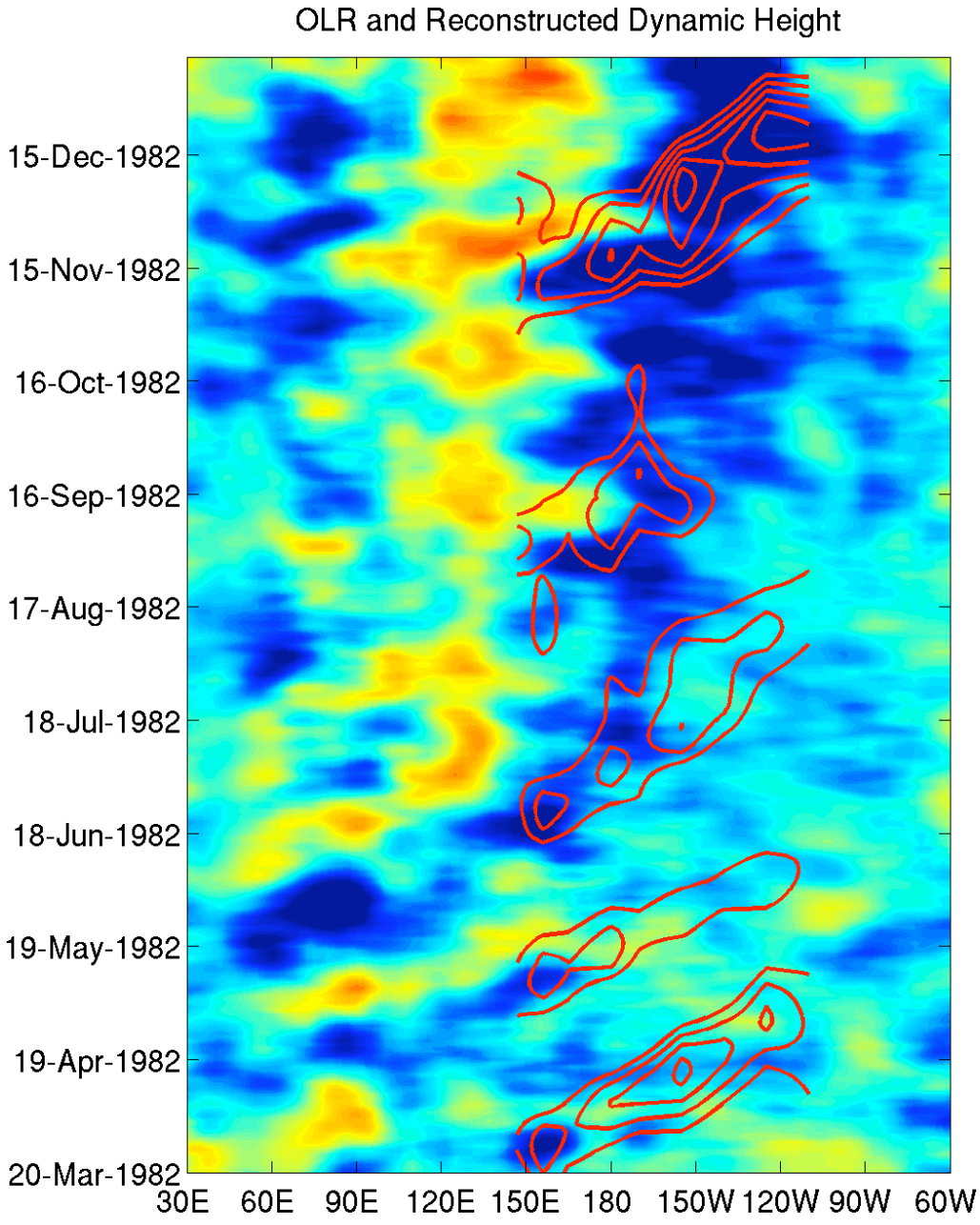

Figure 4 OLR anomaly (shading, blue negative, and the color ranges from -60 Wm^{-2} to +60 Wm^{-2}) and reconstructed dynamic height (positive contours are red, negative contours are blue, with contours every integer cm and the zero contour is omitted) for the period May-December 1982.

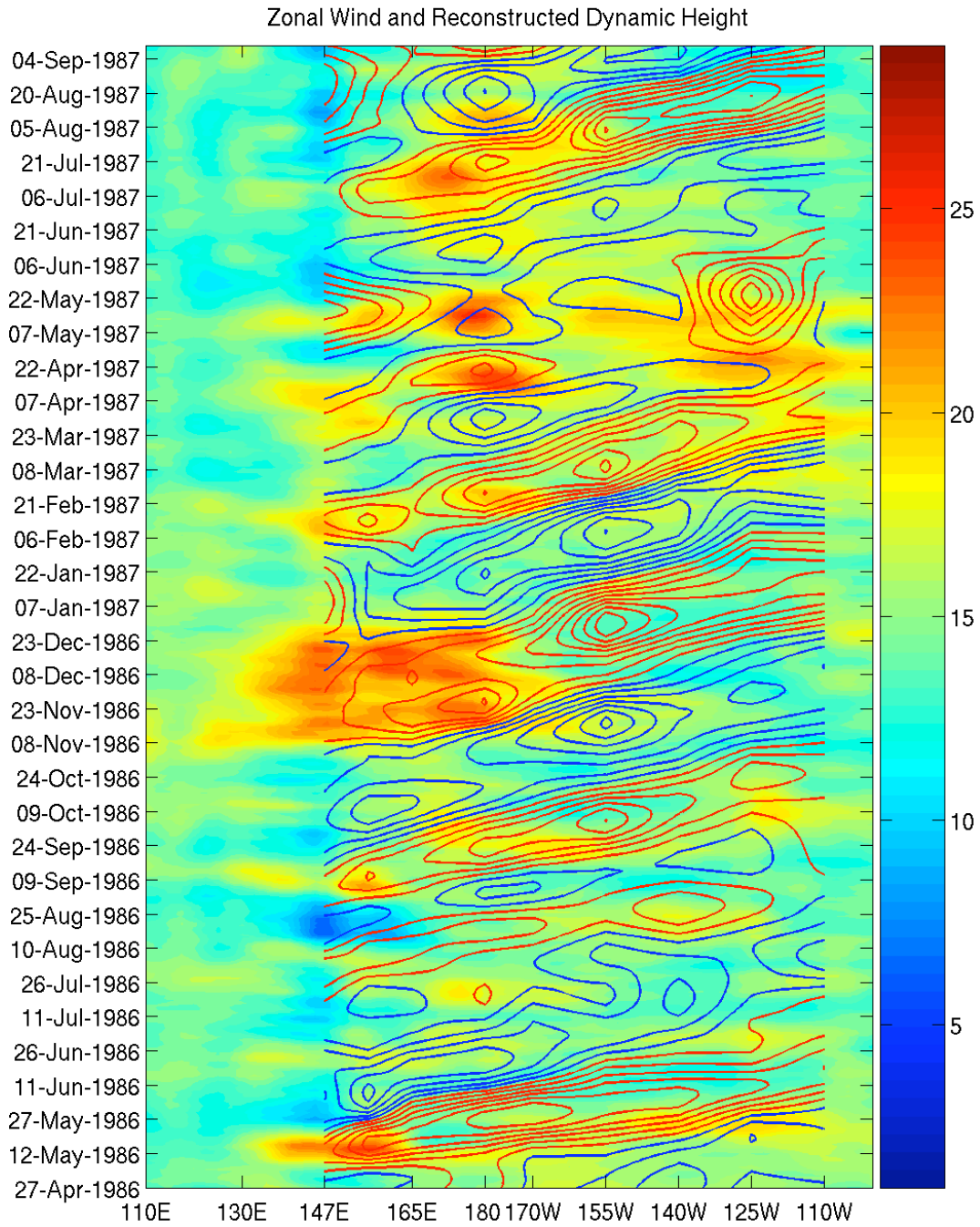

Figure 5 As in Fig. 3, reconstructed dynamic height and zonal wind anomalies for April 27, 1986-September 9, 1987.